Nanoparticle-coated microbubbles for combined ultrasound imaging and drug delivery

Akaki Jamburidze,[†] Axel Huerre,[†] Diego Baresch,[†] Vincent Poulichet,[‡] Marco De Corato,[†] and Valeria Garbin[*,†]

[†]*Department of Chemical Engineering, Imperial College London, London SW7 2AZ, United Kingdom*

[‡]*Department of Chemistry, Ecole Normale Superieure, 75005 Paris, France*

E-mail: v.garbin@imperial.ac.uk

Abstract

Biomedical microbubbles stabilized by a coating of magnetic or drug-containing nanoparticles show great potential for theranostics applications. Nanoparticle-coated microbubbles can be made to be stable, echogenic, and to release the cargo of drug-containing nanoparticles with an ultrasound trigger. This article reviews the design principles of nanoparticle-coated microbubbles for ultrasound imaging and drug delivery, with a particular focus on the physical chemistry of nanoparticle-coated interfaces; the formation, stability and dynamics of nanoparticle-coated bubbles; and the conditions for controlled nanoparticle release in ultrasound. The emerging understanding of the modes of nanoparticle expulsion and of the transport of expelled material by microbubble-induced flow is paving the way towards more efficient nanoparticle-mediated drug delivery. The article highlights the knowledge gap that still remains to be addressed before we can control these phenomena.

Introduction

Biomedical microbubbles find uses in both diagnostic and therapeutic ultrasound.[1,2] Loading of the microbubble coating with nanoparticles is a promising development, as nanoparticles can provide additional functionality to the microbubbles. In addition, several types of nanoparticles can be used as drug carriers, for instance for anticancer drug and gene delivery.[3] For instance magnetic microbubbles are dual agents for magnetic resonance imaging and echography and can be triggered with ultrasound to release the nanoparticle payload.[4,5]

Magnetic microbubbles, which are loaded with iron oxide nanoparticles, have been obtained by various methods belonging to two broad categories: either the nanoparticles are embedded in,[4] or conjugated to,[6] an existing coating; or they can form the coating on the microbubbles.[7,8] Both types of magnetic microbubbles show great promise for imaging and drug delivery. Microbubbles stabilized by a phospholipid coating and subsequently conjugated to magnetic nanoparticles can circulate systemically like commercial contrast agents, and can be accumulated in tumours by magnetic targeting, prior to triggering drug release by ultrasound-induced bubble dynamics. Microbubbles with a coating made of iron oxide nanoparticles and drug-containing nanoparticles were shown to deliver doxorubicin across physiological barriers both *in vitro* and *in vivo*, by driving the microbubbles into stable oscillations instead of using high-pressure pulses to trigger violent bubble dynamics.[9]

New methods to load microbubbles with magnetic or drug-containing nanoparticles are continuously being developed.[10] To aid the development of new theranostic agents, it can indeed be beneficial to innovate the design of microbubbles to achieve the desired performance, as opposed to modifying existing formulations, as Borden & Song recently argued.[11] Modifying existing contrast agents is motivated primarily by the need for regulatory approval, but can impose constraints that continue to limit performance. The example of magnetic microbubbles proves that it is possible to develop formulations that use exclusively nanoparticles, acting simultaneously as stabilizing coating and as payload.[7–9] Such *nanoparticle-coated* microbubbles would simplify manufacturing protocols, and may provide

additional benefits. Some fundamental questions that need to be addressed include how a coating made exclusively of nanoparticles affects stability, performance as ultrasound contrast agents, controlled release of the active pharmaceutical ingredient, and the efficiency of drug uptake.

In this paper we provide a short overview of the design principles of nanoparticle-coated microbubbles and their development as diagnostic and drug delivery agents. We first give a general introduction of diagnostic and therapeutic uses of ultrasound contrast agent microbubbles, highlighting opportunities for nanoparticle-coated microbubbles. We then describe the fundamentals of microbubble stability and microbubble production. Next we cover the phenomena of microbubble dynamics in ultrasound, focusing on the effect of a nanoparticle coating, and highlighting the emerging understanding of the importance of microstreaming flow in drug delivery. Finally we report recent observations of shedding of lipids and nanoparticles from the coating of ultrasound-driven microbubbles.

Microbubbles for diagnostic and therapeutic ultrasound

Several microbubble formulations are clinically approved as contrast agents for ultrasound diagnostic imaging,[11] and increasingly sophisticated imaging strategies have been developed,[12] the most recent one being ultrafast ultrasound localization microscopy,[13] which can detect single echoes from individual microbubbles in microvessels *in vivo* [see Figure 1(a)]. The use of microbubbles in conjunction with ultrasound can increase the efficacy of thrombolysis[15] or reduce acoustic power and treatment time in high-intensity focused ultrasound (HIFU) for tumour ablation.[16] Tight junction opening in the blood-brain barrier has been achieved by the presence of microbubbles under low-power ultrasound.[17] In addition, surface engineering has allowed to use microbubbles as effective tools for localized drug and gene delivery, by functionalizing their coating with targeting ligands and loading them with a payload of drugs.[18] Loading of drugs onto microbubbles has been achieved by three main methods:[10]

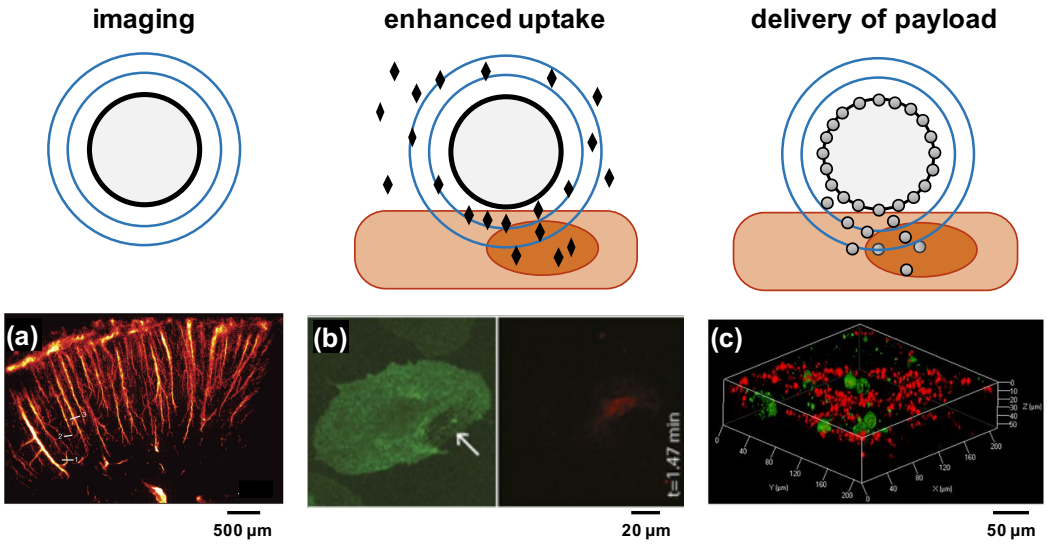

Figure 1: (a) Ultrafast ultrasound localization microscopy of microvessels in rat brain cortex. Reproduced from.[13] (b) 3D confocal microscopy recording of sonoporation, highlighting a large pore in the cell membrane (green channel, left), resulting in uptake of co-administered propidium iodide (red channel, right). Adapted from.[14] (c) Delivery of doxorubicin-containing particles to cells embedded in an alginate hydrogel from ultrasound-driven magnetic microbubbles. Reproduced from.[9]

incorporating an oil layer between the coating and the gas core, incorporating the drug within the coating, or attaching the drug onto the coating. This can be achieved either by electrostatic interactions, since many commercial microbubble formulations have a surface charge,[19] or using bioconjugate chemistry.[20] When drug-loaded microbubbles are exposed to low-pressure ultrasound they act as contrast agents for imaging, while for sufficiently large ultrasound pressure they release their cargo, typically by fragmentation or disruption of the coating due to violent bubble oscillations.[10]

In addition to carrying a payload of drug that can be released using ultrasound, microbubbles also facilitate drug and gene uptake through their interaction with cells. The transient increase in the permeability of a cell membrane due to microbubble activity in ultrasound is termed *sonoporation*, and can be caused by several different mechanisms.[21] It has been demonstrated that a collapsing bubble can induce a temporary pore into the cell membrane which results in the uptake of fluorescent markers or drugs.[14,22] Helfield *et al.*

studied sonoporation *in vitro*.[14] The microbubbles were excited with a short 1-MHz pulse at a relatively high pressure of 0.8 MPa, which was found to cause inertial cavitation. The dynamics of pore formation and resealing of the cell membrane were captured by confocal microscopy [see Figure 1(b)]. The uptake of propidium iodide was monitored to quantify sonoporation activity. Shear stresses of 6-22 kPa due to microbubble inertial cavitation were estimated. In studies of gene transfection, the rates of transfection have been found to increase with ultrasound intensity up to a certain level, after which unwanted effects such as cell death are observed, and the efficiency of the delivery subsequently decreases.[23,24] These unwanted bioeffects are usually attributed to inertial cavitation at high ultrasound pressures, which can cause microbubble collapse, high-speed liquid jets and bubble fragmentation. To avoid microbubble collapse, moderate ultrasound pressures can be employed and drug delivery can still be achieved, as shown by van Wamel *et al.*[25] In this study, 10-cycle bursts of ultrasound at 1 MHz and 400 kPa were applied for a total duration of 5 seconds with a pulse repetition rate of 50 Hz. Two potential mechanisms responsible for increase in the membrane permeability were proposed in this case: the stress directly applied by the oscillating bubble pushing and pulling on the cell membrane, and the shear stress due to the microbbubble-induced microstreaming flow. The shear stresses induced by microstreaming flow have been recently quantified in a dedicated microfluidic device.[26] Sonoporation events were found to coincide with microstreaming flow. For an acoustic pressure of 145 kPa, a shear stress of 1 mPa was quoted at distances of 1 mm away from the bubble. As demonstrated by other studies,[27] the velocity and shear stress decay quickly with distance from the bubble. Values of the stress near the bubble surface may be a better indication of the effect of microstreaming on a nearby cell membrane. Zhou *et al.* quantified the stress applied by a bubble pushing on a cell using laser-generated and trapped microbubbles placed at a controlled distance from a cell membrane.[28] The authors used transmembrane current as the measure of membrane distruption. A bubble pushed by primary radiation force generated a stress of 176 Pa on the cell membrane. The authors argued that the deformation from the

bubble compression was the mechanism for creation of a pore, rather than the stable oscillation of the microbubble. This was supported by the fact that the membrane distruption was observed only after significant deformation of the membrane by the pushing bubble. Endocytosis has also been found to be an important mechanism for uptake, especially for larger molecules.[29] It has been hypothesized that membrane deformation by microbubble oscillations may trigger endocytosis via mechanostimulation of the cytoskeleton.[30]

Recent studies have demonstrated drug delivery from microbubbles loaded with a drug payload,[5,6,9,31] in contrast to the studies described above where a fluorescent marker or drug was co-injected with the microbubbles. Nanoparticle-loaded microbubbles are an example. Nanoparticle-loaded microbubbles can be triggered by ultrasound to deposit nanoparticles directly on a cell, by a mechanism that has been termed *sonoprinting* and which was found to significantly enhance cellular delivery.[31] Delivery of nanoparticles into hydrogels [Figure 2(c)] and animal models has been demonstrated with low-pressure ultrasound.[9] Nanoparticle-coated microbubbles therefore hold promise for controlled drug delivery and enhanced uptake without unwanted bioeffects.

Microbubble stability

We now turn our attention to the physico-chemical underpinnings of the design and manufacture of coated microbubbles. An important requirement for biomedical microbubbles is that their size be sufficiently small for safe intravenous injection. Typical sizes are between 2 and 8 μm in diameter, smaller than red blood cells. Bubbles larger than 10 μm are filtered by the lungs and can be responsible for embolism.[32–34] The first commercially available contrast agent was an albumin-coated, air-filled microbubble.[35] Most of the microbubble formulations currently available comprise coatings made of denatured albumin or phospholipids,[36] and gas cores made of low-solubility, inert gases, such as perfluorocarbon gas and sulphur hexafluoride.[37] The choice of coating material and gas are guided by the

need for microbubbles to be stable against dissolution, as explained in the following.

Thermodynamics and mechanics of coated interfaces

The interface between a gas and a liquid is characterized by the surface tension, σ, representing the energy per unit area required to form the interface. For stationary, spherical bubbles, the surface tension generates an extra pressure in the gas that is inversely proportional to the bubble radius, R, and proportional to the surface tension: $\Delta p = 2\sigma/R$. The extra pressure inside the bubble due to surface tension is called Laplace pressure and acts as a driving force for the diffusion of the gas into the liquid phase. The Laplace pressure increases with decreasing bubble radius and is of the same magnitude as the ambient pressure for micron-sized bubbles, leading to complete dissolution in tens of milliseconds.[38]

To reduce the surface tension and therefore the driving force for dissolution, it is possible to exploit the adsorption of surfactants, proteins, nanoparticles or other surface-active species. For formulations of biomedical microbubbles, insoluble surfactants such as phospholipids are usually selected, which adsorb irreversibly at the gas-water interface and have negligible solubility in water. The surface-active species form a monolayer at the gas-liquid interface, which acts as a coating on the bubble. The effective surface tension of a coated bubble interface is a function of the surface concentration of the adsorbed species, $\Gamma = n^{\mathrm{s}}/A$, where n^{s} is the number of moles of adsorbed species and A the surface area.

When the surface of the bubble is deformed from its equilibrium shape, the interfacial coating generates additional stresses compared to the case of a simple gas-liquid interface. Both the change of surface tension and the emergence of interfacial stresses are the macroscopic manifestation of the interactions between the molecules or particles adsorbed at the interface, and can vary depending on the constituents forming the monolayer. The mechanical response of interfacial coatings can be very complex.[40] Here we focus on the behavior and the stability of spherical coated bubbles that expand and compress, thus changing the surface area and volume without changing shape. In this case, the interface undergoes a purely

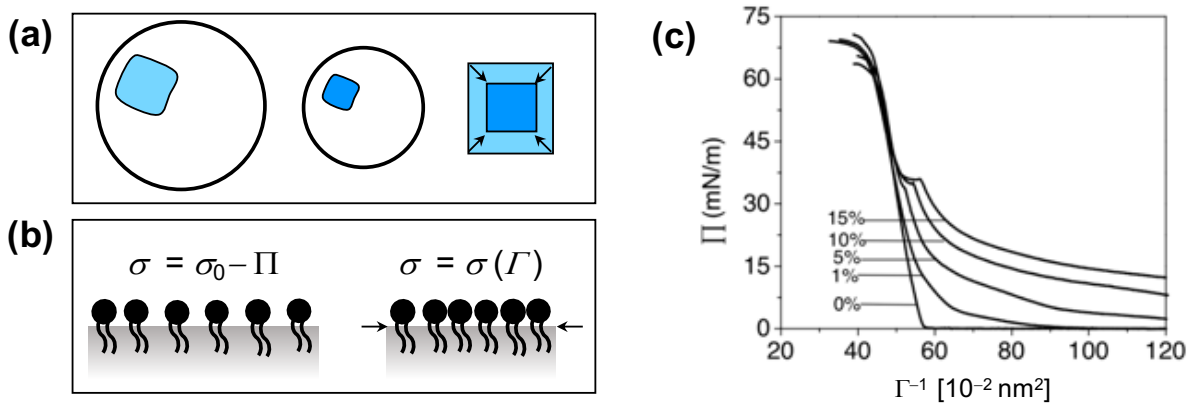

Figure 2: (a) Purely dilatational deformation of the interface of a spherical bubble undergoing volumetric oscillations. (b) The effective surface tension σ of a gas-liquid interface coated with surfactants is lower than the surface tension of the bare interface, σ_0. The difference, Π, is termed surface pressure. These quantities depend on the surface concentration of surfactant, Γ. (c) Surface pressure-area isotherms for monolayers of di$C_{18:0}$PC lipids with different content of PEG40S emulsifier ($0 - 15\%$). Γ^{-1} is the area per molecule. Adapted from.[39]

dilatational deformation, as shown in Figure 2(a). The shear response of the monolayer[41] is relevant in the case of non-spherical deformation, which will not be discussed here.

For molecules or particles that are irreversibly adsorbed to the interface (called Langmuir monolayers), the surface concentration of material, Γ, changes during compression/expansion of the bubble, because of reduction/increase of the surface area. As a consequence, the effective surface tension changes with the change of surface area, $\sigma = \sigma(A)$. Langmuir monolayers can be characterized by depositing them on a water subphase and compressing/expanding the area A so as to increase/decrease the surface concentration Γ (at constant number of moles n^{s}). Typically the quantity measured is the surface pressure Π, defined from $\sigma = \sigma_0 - \Pi$, with σ_0 the surface tension of the bare gas/liquid interface and σ the effective surface tension in the presence of the monolayer [Figure 2(b)]. A surface pressure-area isotherm (Γ^{-1} gives the area per molecule) is shown in Figure 2(c) for di$C_{18:0}$PC lipids with different content of PEG40S emulsifier.[39]

The mechanical property describing the elastic response of the interface during dilata-

tional deformation is the interfacial dilatational elasticity, or surface compression modulus, defined as:

$$E^{\mathrm{s}} = A\frac{\mathrm{d}\sigma}{\mathrm{d}A}, \tag{1}$$

at constant mass of material on the interface. The interfacial dilatational elasticity has the same dimensions as the surface tension and can be obtained, in the quasi-static limit, from surface pressure-area isotherms. This interfacial mechanical property, originally known in the context of surfactants, has been introduced in the modelling of ultrasound contrast agents.[42] In this case, the dilatational elasticity at the high frequency of deformation characteristic of ultrasonic driving can differ significantly from that measured in the quasi-static limit, as rheological properties of complex fluids and interfaces depend on the rate of deformation.[40] The molecular and microstructural rearrangements underlying changes in mechanical response at high deformation rates remain the subject of ongoing research.

During dynamic deformation of the interface, the intermolecular forces within the monolayer also cause some dissipation of energy. This dissipation can be taken into account through a surface dilatational viscosity,[43] κ^{s}. When the interface is expanded or compressed, the coating experiences a viscous stress that resists the deformation and is proportional to the product of the dilatation rate and of the dilatational viscosity. These elastic and viscous stresses contribute to the extra pressure inside the bubble in the dynamic case. For a spherical, coated bubble of radius R, the jump in pressure at the gas-liquid interface is given by:

$$\Delta p = 2\frac{\sigma(A)}{R} + 4\kappa^{\mathrm{s}}\frac{\dot{R}}{R^2} + 4\eta\frac{\dot{R}}{R}, \tag{2}$$

where the dot denotes derivative with respect to time. In Equation 2, the interfacial dilatational elasticity of the monolayer is taken into account through the dependence of the surface tension on the instantaneous surface area of the bubble. The term $4\kappa^{\mathrm{s}}\dot{R}/R^2$ represents the viscous stress due to the compression/expansion of the monolayer at a rate $\dot{R}/R$. The last term on the right-hand side of Eq. (2) represents the bulk viscous stresses due to

the surrounding liquid of viscosity η, and is present also for a pure gas-liquid interface in the dynamic case.

Knowledge of the interfacial properties is important for determining the stability of bubbles coated with monolayers of molecules or particles, as we will see next. In addition, the mechanical properties of the interfacial coating also have important effects on the bubble dynamics in ultrasound, as will be discussed in a later Section.

Stability against dissolution

The need for microbubble formulations that remain stable against dissolution has led to the development of different strategies to limit this effect. Gases that are poorly soluble in water, like perfluorocarbons and sulphur hexafluoride,[37] are typically used. The equation governing the dissolution of small spherical bubbles[44] highlights the role of the Laplace pressure:

$$\dot{R} = -Dk_{\mathrm{H}}BT\left(1 - f + \frac{2M}{\rho_0 BT}\frac{2\sigma}{R}\right)\left(1 + \frac{2M}{3\rho_0 BT}\frac{2\sigma}{R}\right)^{-1}\left(\frac{1}{R} + \frac{1}{\sqrt{\pi Dt}}\right). \tag{3}$$

In Equation 3, describing the rate of change of bubble radius with time under the assumption of an ideal gas, D is the diffusivity of the gas in the liquid, k_{H} is the Henry's constant (solubility) of the gas in the liquid, B is the universal gas constant, T is the absolute temperature, f is the gas saturation level in the liquid, M is the molecular weight of the gas, ρ_0 is the density of the gas at ambient pressure, and σ is the surface tension. The saturation level is defined as $f = c_{\mathrm{i}}/c_{\mathrm{s}}$, where c_{i} is the initial concentration of gas dissolved in the liquid, and c_{s} the saturation concentration, related to the partial pressure, p_{gas}, of a gas phase in equilibrium with the liquid through Henry's law, $c_{\mathrm{s}} = k_{\mathrm{H}}p_{\mathrm{gas}}$. The equation shows that even when the liquid is saturated with gas ($f = 1$) the Laplace pressure continues to drive bubble dissolution.

The presence of an interfacial coating on a bubble can help to slow down and even arrest dissolution due to the Laplace pressure. There are three main contributing factors for the

stabilization of bubbles by adsorbed molecules or particles. First, a reduction in the effective surface tension σ helps to stabilize bubbles since the pressure difference Δp decreases.[45,46] Second, the gas permeation across the interface can be reduced due to steric effects, caused by the physical barriers from the adsorbed molecules/particles.[47,48] The decrease in gas permeation is particularly effective when a high-molecular-weight gas, such as perfluorocarbon, is encapsulated in a dense lipid coating.[49] Third, the mechanical properties of the interfacial coating can completely arrest bubble dissolution, provided that the interfacial dilatational elasticity, E^{s}, is above a certain threshold.[50,51] This threshold can be derived from the change in Laplace pressure Δp with the bubble radius R:

$$\frac{\partial(\Delta p)}{\partial R} = -\frac{2\sigma}{R^2} + \frac{2}{R}\frac{\partial \sigma}{\partial R} = \frac{2}{R^2}(2E^{\mathrm{s}} - \sigma), \tag{4}$$

where we have used Eq. 1 to write $E^{\mathrm{s}} = A\frac{\partial \sigma}{\partial A} = \frac{R}{2}\frac{\partial \sigma}{\partial R}$. When $E^{\mathrm{s}} > \sigma/2$, the change in Laplace pressure, $\frac{\partial(\Delta p)}{\partial R}$, is negative, and bubble dissolution slows down until it is arrested. This criterion has been shown to be satisfied for bubbles stabilized solely by nanoparticles.[51] Furthermore, a possible stabilisation mechanism has been proposed in the context of bulk nanobubbles, where hydrophobic patches are already sufficient to arrest dissolution.[52] Since nanoparticles can impart outstanding stability to bubbles, new formulations could be designed that exhibit the necessary stability for applications in diagnostic ultrasound.

Production of microbubbles

In the past 40 years, different strategies have been used to produce microbubbles suitable for biomedical applications. This requirement yielded several approaches in order to control both the size distribution and the stability of the produced microbubbles, which have been reviewed in.[53] Here we summarize only a few of the existing methods, with a focus on the methods that can be applied to the preparation of nanoparticle-coated microbubbles.

From polydisperse to monodisperse microbubbles

Historically, two main strategies have been used to massively produce microbubbles in a stochastic way.[54] The first one uses simple mechanical agitation. A solution of the surface-active species used to stabilize the bubbles is sealed in a vial and then agitated with a shaking machine.[55] Doing so, gas is entrained into the liquid and microbubbles are produced. The second one, the ultrasonication method, is based on a cavitation process. The solution is placed into a container subjected to a strong acoustic field, usually by immersing the tip of a sonicator horn in the bath. This yields to cavitation and the creation of microbubbles.[56–59] The main advantages of these techniques are their high throughput and their low cost of production. More recently developed methods include coaxial electrohydrodynamic atomization[60] and pressurized gyration.[61] The obtained microbubbles typically have a broad size distribution. Several strategies have been employed to obtain a narrower size distribution by eliminating unwanted microbubbles, for example buoyancy separation and fractionation,[59] differential centrifugation,[62] flow fractionation[63] [see Figure 2(a)], or acoustic sorting.[64] Although narrow size distributions are attainable through sorting methods, their throughput remains limited.

Microfluidic devices are ideal for producing monodisperse populations of microbubbles, and have now reached sufficiently high throughputs.[53,65–67] Two main geometries are used to produce monodisperse microbubbles of controlled size: T-junctions[68] and flow-focusing devices.[69] In a T-junction [see Figure 2(b)], a gas thread is produced into a straight channel containing the flowing solution of surfactants.[68,70,71] For a certain set of parameters, the gas is pinched and breaks regularly into bubbles. The bubble size is set by the geometrical parameters of the junction but also by the ratio of the flow rates, allowing for the production of different bubble sizes with the same system. A simple T-junction device can produce microbubbles at a frequency of 7.5 kHz.[72] In a flow-focusing device [Figure 2(c)], a gas thread is pinched by two lateral flows of surfactant solution.[69] The gas is forced to go through a constriction which triggers an instability and the controlled breaking of the gas thread into

microbubbles. There are several regimes in which a flow focusing chip can be operated, which affect the size of the bubbles produced, their polydispersity and the production rate. Production rates from a flow-focusing device as high as 1 MHz have been measured.[73] Using parallelized flow-focusing devices, a usable batch (10^{10} microbubbles/mL) can be produced in 10 min.[74] This performance compares well with sonication throughput (2 min of ultrasound and 10 min of size separation) for similar concentrations of microbubbles.[59] Parallelization is however not a straightforward approach, as crosstalk and slight differences between channels can induce a significant increase in polydispersity and require refined designs to be applicable. Some variations of these strategies of microbubble production include the co-flowing junction[75] and the liquid cross flow.[76]

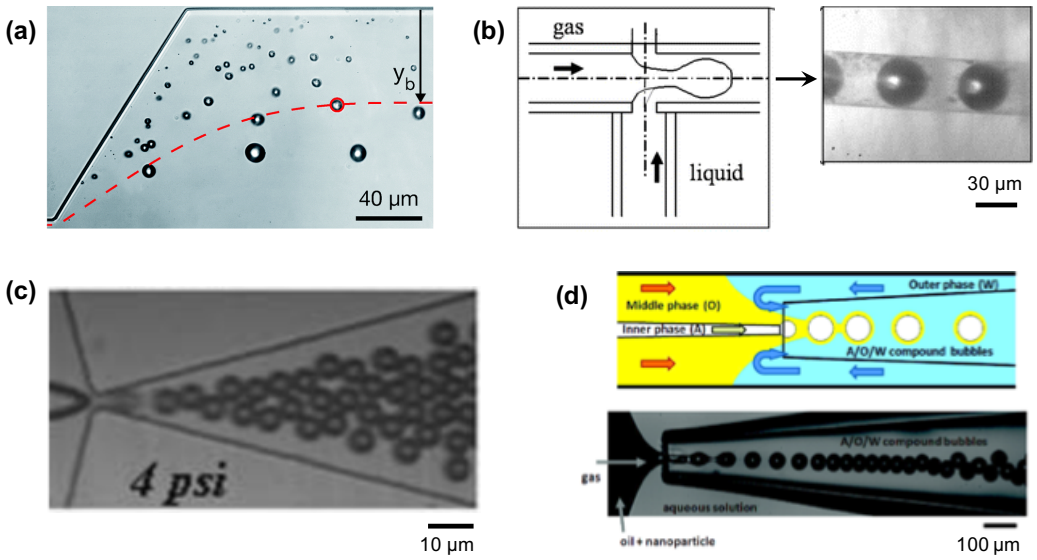

Figure 3: Methods for production of monodisperse microbubbles. (a) Bubble sorting by flow fractionation. Reproduced from.[63] (b) T-junction geometry. Adapted from.[77] (c) Production of monodisperse ultrasound contrast agent microbubbles with a flow-focusing device. Reproduced from.[73] (d) Coating of microbubbles with nanoparticles using a temporary oil layer under flow in a capillary. Reproduced from[78]

.

Nanoparticle-coated microbubbles

Methods to produce bubbles stabilized solely by nanoparticles must overcome the challenges of adsorbing solid particles at interfaces. Solid particles with homogeneous surface properties adsorb to a given gas-liquid interface only if their wettability (in terms of the three-phase Young's contact angle) is favorable.[79] In addition the size of the particles can be large (10-100 nm) compared with phospholipids (about 2 nm), making their diffusivity lower. In microfluidics, where mixing occurs only by diffusion, this can limit the amount of particles that adsorb to a newly created microbubble. Different strategies have been devised to create coatings of nanoparticles on the surface of microbubbles.[80] One possible route is to use a temporary phase (usually an oil phase) to create a "double emulsion" under flow in capillaries [see Fig. 3(d)]. The nanoparticles are carried in the oil phase that is positioned between the air and the water when creating the air-in-oil-in-water "emulsion". A final step of oil removal allows for the attachment of the nanoparticles at the microbubble surface.[78] Adsorption has been achieved in microfluidics by simply flowing bubbles produced at a T-junction in a solution containing the nanoparticles.[81,82]

An alternative approach to stabilizing bubbles with nanoparticles is to load the surface of a lipid-coated bubble with nanoparticles, by controlling the electrostatic interaction between the nanoparticles and the coating.[83] This method was proved successful for silica-coated nanoparticles and has been implemented in microfluidics, with the added advantage of monodisperse bubble production while preserving a high throughput (10^6 microbubbles/s). Sonication has also been used to produce large quantities of microbubbles stabilized both by phospholipids and nanoparticles.[84] Another approach which shows promise for preparing monodisperse microbubbles was demonstrated by integrating oscillating electric fields with a microfluidic T-junction.[85]

Microbubble activity in ultrasound

Microbubbles scatter ultrasound waves more effectively than blood and tissues, due to the high compressibility mismatch between the gas core and the surroundings. Due to the compressibility of the gas core, microbubbles oscillate, thereby emitting detectable secondary sound waves. The resonance frequencies of microbubbles by a fortunate coincidence lie in the range of frequencies used in diagnostic ultrasound (2-10 MHz). The incorporation of a payload of nanoparticles within or onto the coating affects the microbubble response in ultrasound. Predictive models of the change in resonance frequency and amplitude of oscillations can guide the design of nanoparticle-loaded microbubbles that remain effective as ultrasound contrast agents. In this section we review the basic theory of bubble dynamics in ultrasound and briefly discuss the effect of an interfacial layer and the flow generated by bubble oscillations. A detailed review of different models for the dynamics of coated bubbles can be found in Ref.[86]

Dynamics of coated microbubbles

The pressure change associated with the propagation of ultrasound, $p_\infty = p_0 + p_A(t)$ where p_0 is the ambient pressure, drives successive cycles of compression and expansion of the bubble volume, $V(t)$. For moderate acoustic forcing, $|p_A| < p_0$, a bare bubble will retain its spherical shape and the dynamics is simply described by the time-dependent bubble radius, $R(t)$. The ordinary differential equation that governs the radius evolution in time of a bubble in an infinite incompressible liquid medium is given by the famous Rayleigh-Plesset equation:[87]

$$\rho\left(R\ddot{R} + \frac{3}{2}\dot{R}^2\right) = p_{\text{gas}} - p_\infty - \frac{2\sigma}{R} - \frac{4\eta\dot{R}}{R}, \tag{5}$$

where ρ and η are respectively the fluid's density and shear viscosity, p_{gas} is the pressure of the gas contained in the bubble and the dot denotes the derivative with respect to time. The pressure change inside the bubble is modelled by $p_{\text{gas}} = p_{\text{gas},0}(R_0/R)^{3\kappa}$ where κ is an effective

polytropic coefficient and $p_{\mathrm{gas},0} = p_0 + 2\sigma/R_0$ is the bubble pressure at rest with equilibrium radius R_0. The polytropic coefficient κ varies between 1 and the ratio of the specific heats at constant pressure and constant volume of the gas when isothermal or adiabatic processes are considered respectively.[88]

When the acoustic pressure, $p_A(t) = P_A \sin(2\pi f t)$ where f is the frequency, is of sufficiently small amplitude, P_A, in order to assume a linear deviation of the bubble radius, $R(t) = R_0[1 + x(t)]$ with $|x(t)| \ll 1$ from its radius at rest, R_0, the linearization of Eq. (5) gives:

$$\ddot{x} + 2\beta\dot{x} + \omega_0^2 x = -P_A \sin(\omega t)/\rho R_0^2 \qquad \text{with} \quad \omega = 2\pi f, \tag{6}$$

$$\text{and} \qquad \omega_0^2 = \frac{1}{\rho R_0^2}\left(3\kappa p_0 + \frac{2(3\kappa - 1)\sigma}{R_0}\right). \tag{7}$$

Hence, a bubble undergoing gentle radial oscillations can be analyzed by analogy with a damped harmonic oscillator, where the mass corresponds to that of the liquid displaced by the bubble interface and the restoring spring constant corresponds to the compression of the gas core and surface tension.[89] The natural frequency of the bubble is given by ω_0. The only damping mechanism included in Equations (5)-(7) involves viscous forces exerted by the surrounding fluid and the damping coefficient is simply given by $\beta = \beta_{\mathrm{vis}} = 2\eta/\rho R_0^2$. The acoustic radiation of spherical waves in actual fluids and heat conduction in the gas will contribute to the total oscillation damping process and β will generally by a sum of all three contributions.[88]

A first approach to understand the effect of a coating on the bubble dynamics consists in assuming that the coating monolayer behaves as a thin, continuous, elastic shell. De Jong *et al.*[90] investigated the linear scattering and absorption cross sections of albumin encapsulated microbubbles. A shift of the resonance to higher frequencies was measured, allowing for an extrapolation of the effective shell stiffness of the protein coating introduced in the expression of ω_0. In developing a Rayleigh-Plesset-type equation for encapsulated

bubbles,[91] Church gave a general theoretical framework to study their linear and nonlinear dynamics. Ascribing, *ad hoc*, an effective shell rigidity (affecting the resonance frequency ω_0) and internal viscosity (affecting the damping β) is however limited by the strong assumption of shell continuity.

Sarkar and co-workers first introduced the use of an interfacial rheological model to describe the effect of the molecular monolayer on ultrasound contrast agent microbubbles.[43] They then introduced the dilatational elasticity of the monolayer[42] to describe the variation of the surface tension with the bubble area, $\sigma(A)$, which can be related to the change in radius:

$$\sigma(R) = \sigma(R_0) + E^{\mathrm{s}} \left(\frac{R^2}{R_0^2} - 1 \right), \tag{8}$$

with E^{s} the surface dilatational elasticity. In an effort to better understand some nonlinear behaviors of ultrasound contrast agents, Marmottant *et al.*[92] considered the realistic behavior of a phospholipid monolayer upon area compression [see Figure 1(c)]. In this model, Equation 8 is only valid in a narrow range of bubble radii (linear regime). Below a minimum bubble radius, the monolayer is assumed to buckle, leading to an abrupt change of the surface tension to zero. Beyond a critical rupture radius, the monolayer ruptures, exhibiting large portions of bare gas/water interface. The surface tensions is then assumed to evolve towards that of the gas/water interface. Combining Equation 2 and Equation 5, an equation governing the dynamics of coated bubbles is obtained:[42,92]

$$\rho \left(R\ddot{R} + \frac{3}{2}\dot{R}^2 \right) = \left(p_0 + \frac{2\sigma(R_0)}{R_0} \right) \left(\frac{R_0}{R} \right)^{3\kappa} - p_0 - p_A(t) - \frac{2\sigma(R)}{R} - \frac{4\eta\dot{R}}{R} - \frac{4\kappa_s\dot{R}}{R^2}, \tag{9}$$

with κ_s the surface dilatational viscosity. Linearization of Equation 9 returns the natural frequency of a coated bubble:[93]

$$\omega_0^2 = \frac{1}{\rho R_0^2} \left(3\kappa p_0 + \frac{2(3\kappa - 1)\sigma}{R_0} + \frac{4E^{\mathrm{s}}}{R_0} \right). \tag{10}$$

valid for oscillation of small amplitude in the linear regime, that is, for radii between the buckled and ruptured states described above. As nanoparticle monolayers can be characterized with the same methods used for phospholipid monolayers, the dependence of surface tension on area, $\sigma(A)$, can be measured to obtain the surface dilatational elasticity E^{s}, albeit at low strain rates compared with the frequency of ultrasound-driven deformation. Upon area compression, monolayers of nanoparticles at the air/water interface have been found to buckle, much like phospholipid monolayers.[94] The model presented in Equations 8-9 for phospholipid-coated bubbles could therefore be used to describe the dynamics in ultrasound of nanoparticle-coated bubbles. The applicability of the model to nanoparticles has not yet been validated experimentally. Finally, instead of buckling, nanoparticles can also be expelled from an interfacial monolayer upon area compression,[79,94] providing a mechanism for payload delivery, as discussed below.

Non-spherical oscillations

Whereas during small-amplitude oscillations the bubble will remain spherical, two frequently encountered situations can give rise to non-spherical oscillations. The first, which is of practical importance for *in vitro* and *in vivo* applications, is when a bubble oscillates nearby a rigid or compliant boundary. The asymmetric flow generated by the oscillations in the presence of the boundary can force a perturbation of the bubble surface and trigger specific surface modes at the driving frequency. The second, that usually appears for a stronger forcing, is when an initial small perturbation of the bubble surface grows during the compression-expansion cycles through a parametric instability, giving rise to shape oscillations. The threshold in acoustic pressure for shape oscillations depends on the frequency, and is a minimum when the bubble is driven close to the natural frequency for spherical oscillations,[95] ω_0. The parametric instability occurs for a driving frequency $\omega = 2\omega_n$, with ω_n the resonance

frequency of a spherical harmonic mode of order $n > 1$, given by Lamb's equation:

$$\omega_n^2 = \frac{(n-1)(n+1)(n+2)\sigma}{\rho R_0^3}. \tag{11}$$

Because of the condition for parametric instability, shape oscillations driven at a frequency ω exhibit subharmonic behaviour with frequency $\omega_n = \omega/2$. Experiments on uncoated bubbles show mode selectivity depending on the bubble radius, R_0, consistent with Eq. 11, and subharmonic behaviour. Shape oscillations of phospholipid-coated microbubbles have been found to display a subharmonic behavior, but without shape mode selectivity.[96] Finally, shape oscillations of nanoparticle-coated bubbles have also been reported.[97] Like for phospholipid-coated bubbles there is subharmonic behavior but no mode selectivity. In the next Section we will discuss how the shape of non-spherical bubbles directs the expulsion of interfacial material. A suitable modification of Eq. 11 may predict the mode of shape oscillations of coated bubbles. In the future, such a development may enable to exploit shape oscillations in a controlled fashion for drug delivery.

Microstreaming flow

The flow generated by microbubble activity in ultrasound affects the transport of therapeutic material present in the surrounding fluid, and plays an important role in enhanced drug uptake in cells. Here we describe the origin and characteristics of the net flow generated by oscillating microbubbles in contact with boundaries, and some observed bioeffects.

Acoustic streaming is a net flow that arises as a consequence of momentum dissipation occurring in viscous fluids.[98] To first order, the linear propagation of sound does not support the existence of a steady flow, since all the relevant quantities (density, particle velocity and pressure) are described as small oscillations around their respective value at rest. The steady flow appears as a second order, nonlinear effect that emerges from the dissipation of the primary, linear oscillating flow. An important consequence is that a doubling of the

oscillation amplitude increases the final speed of the steady flow four-fold. Here we are interested in one particular class of steady flow, termed acoustic microstreaming,[99] where the flow patterns and emerging stresses take place in a microscopic length scale. Oscillating microbubbles have been recognized to generate steady circulation patterns in the bulk originally described by Elder.[100] The dissipation occurs within a thin viscous boundary layer of thickness, $\delta = (2\eta/\omega)^{1/2}$, appearing around any oscillating boundary.[101] Typically, for ultrasound in the low MHz range in water, we have $\delta \sim 1\mu$m. The time, τ, necessary to fully develop the steady flow is much larger than the primary oscillation period, $T = 2\pi/\omega$. Hence microstreaming becomes clearly appreciable after a large number of oscillations, $N \sim 10^3$, such that $\tau = NT \sim 1$ ms for MHz ultrasound.

The case of relevance to biomedical applications of a bubble in contact with a boundary combines radial oscillations and translation of the center of mass of the bubble. Advanced optical techniques using particle tracking in 3D have revealed the detailed features of the resulting flow patterns.[27] The particles are alternatively repelled from the bubble surface and attracted, as they are transported along closed streamlines. The flow velocity is maximum near the bubble and decreases over a distance of a few bubble radii. When both the radial oscillations and vertical translation of the bubble are of the same order of magnitude, given by ϵR_0 with $\epsilon \ll 1$, the maximum fluid velocity close to the bubble is approximately $u \sim \epsilon^2 a\omega$ and can reach several mm/s. Because the flow speed is directly proportional to the square of the oscillation magnitude, bubbles excited close to their resonant frequency will efficiently force strong flows.

If the bubble undergoes non-spherical oscillations in stronger pressure fields, the resulting flow pattern can be significantly modified.[100] In particular, the large surface displacement at the antinodes of a shape oscillation mode, which can be approximately one order of magnitude greater than the typical radial displacement during a volume oscillation cycle, can enhance the total mass transfer in the vicinity of the bubble surface.[102] This enhanced streaming regime is known to be difficult to control in experiment[103] and requires further

investigation for it is important in particle release and transport discussed below.

The viscous stresses developed in microstreaming flows are of critical importance for acoustically induced bioeffects, as discussed above for the case of enhanced drug delivery. Rooney originally showed that the flow shear rate is directly linked to the rate of hemolysis.[104] Marmottant and Hilgenfeldt also reported on the lysis of lipid vesicles, suggesting an important role for microstreaming in the process of sonoporation.[105] It was also shown that it is possible to tune the lysing power of microbubble-induced microstreaming depending on the different mechanical resistances of vesicles with different composition.[106] The evidence for bioeffects induced by microstreaming flow is still limited compared with the case of bubble collapse. A better understanding of this mechanism is required for it to be exploited in a controlled fashion. The steady flow generated by oscillating microbubbles in the vicinity of cells is not only important because of the induced bioeffects, but also in relation to transport of material expelled from the coating of microbubbles, which is discussed in the next Section.

Expulsion of interfacial material

Many studies on microbubble-enhanced drug uptake have been performed using a mixture of microbubbles and drug molecules (or fluorescent markers as model molecules, in order to visualize the uptake). Microbubbles loaded with nanoparticles on their coating have been shown to improve delivery to cells relative to co-administration.[31] The mechanisms that have been proposed to explain this observation include the localized, high concentration of drug, and enhanced transport due to microbubble-generated flow. For microbubbles loaded with either drug molecules or nanoparticles, our knowledge of how the microbubble-bound material is released and taken up by the cell is still limited. Direct observations of how phospholipids[107,108] and nanoparticles[9,97,109] are expelled from the coating of ultrasound-driven bubbles are beginning to cast light on the conditions for expulsion in different regimes of bubble dynamics, and on the role of microbubble-induced flow on the transport of expelled

material. An important, common feature of these studies is the possibility to release a payload in a controlled manner and at low acoustic pressure.

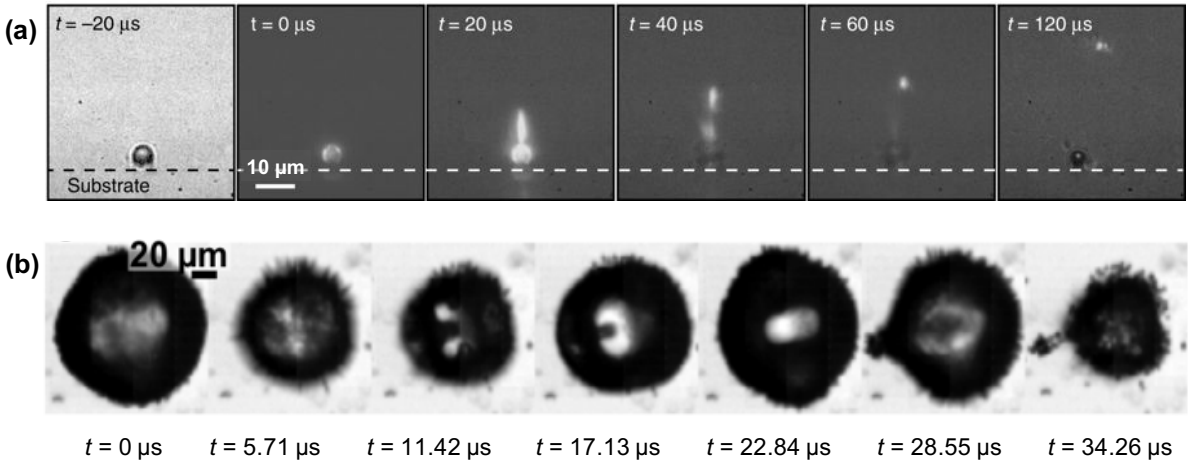

Figure 4: Expulsion of interfacial material from ultrasound-driven, coated bubbles. (a) Shedding of fluorescently labelled lipids from ultrasound contrast agent microbubble and transport of the expelled material in the microstreaming flow generated by the bubble. Reproduced from.[108] (b) Bubble stabilized by 1-μm particles undergoing collapse and jetting. A directional plume of particles is expelled with the jet. Reproduced from.[109]

Buckling of the lipid monolayer and lipid shedding from microbubbles undergoing slow deflation has been well known already for 15 years.[45] It was later shown that buckling is possible also during the high-rate compression of bubbles at ultrasound frequency.[110] More recently, using high-speed fluorescence imaging, it has been possible to visualize the dynamic shedding of fluorescently labelled lipids from contrast agent microbubbles during ultrasonic driving.[107] The ultrasound parameters consisted of a single burst of 20-1000 cycles at a frequency of 1 MHz and acoustic pressures of 50 to 425 kPa. The threshold for lipid shedding was found to be $0.3R_0$, and was ascribed to the bubble surface area reduction during compression. Figure 4(a) shows the transport of the ejected lipids in the microstreaming flow generated by the the bubble dynamics,[108] with typical velocities of the order of 0.1 m/s.

For particle-coated bubbles, different phenomena leading to particle expulsion have been reported depending on the amplitude of oscillations: buckling of the monolayer followed by expulsion for small amplitude;[109] shape oscillations and directional particle expulsion for

larger amplitude.[9,97] Interestingly, for non-spherical oscillations the shape of the bubble can cause directional expulsion of the particles. Figure 4(b) shows an example where a bubble undergoing collapse and jetting generates a directional plume of ejected particles.

Particle-coated bubbles are a useful model system to understand the mechanism leading to expulsion of interfacial material. Once a particle adsorbs at a fluid interface, it can be considered to be irreversibly adsorbed since the change in free energy ΔF is very large.[111] The adsorption energy ΔF writes:

$$\Delta F = -\pi a^2 \sigma (1 - \cos\theta)^2, \tag{12}$$

where a is the particle radius and θ is the contact angle that the particle makes with the interface. For particles of radius 10 nm, this energy can be of the order of $|\Delta F| \sim 10^3\ k_\mathrm{B}T$, with $k_\mathrm{B}T$ the thermal energy. Two modes of particles expulsion have been identified that correspond to the two different regimes of bubble dynamics. First, for small amplitude driving ($\Delta R/R_0 < 0.1$) the desorption is attributed to the interfacial compression. When the bubble's volume decreases, the surface area available per particle decreases. This causes the surface pressure Π of the particle monolayer to increase until the work done on a particle overcomes its adsorption energy. The work done on the monolayer upon compression can be estimated as $W = \Pi dA$, where dA is the change in area. The condition for particle expulsion during small amplitude oscillations can then be written as:

$$\frac{W}{\Delta F} = \frac{\Pi}{\sigma(1 - \cos\theta)^2} > 1. \tag{13}$$

Surface engineering of nanoparticles can therefore be used to design coated microbubbles that release nanoparticles in a desired range of conditions, for instance for smaller or larger amplitude of oscillations depending on the magnitude of ΔF.

When a particle-coated bubble undergoes shape oscillations, the observed patterns of expelled particles that depend on the bubble shape point to a second desorption mechanism:

the large kinetic energy of the particles at the antinodes, where the velocity of the interface is a maximum, exceeds the adsorption energy ΔF. Because particle expulsion is directional and localized at the antinodes, it is attractive to attempt to exploit this phenomenon to "inject" particles into cells. A demonstration has been provided for magnetic microbubbles including doxorubicin-containing particles, which were delivered across a physiological barrier both *in vitro* and *in vivo*.[9]

Conclusions and perspectives

Nanoparticles alone can be sufficient to stabilize microbubbles, while also acting as the payload. Nanoparticles that self-assemble at the gas-liquid interface can provide effective stabilization, while on the other hand it has to be possible to remove the particles from the interface with an ultrasound trigger for payload delivery. Several demonstration exist, but more fundamental research in colloid and interface science will underpin the formulation of nanoparticle-coated microbubbles with a variety of therapeutic nanoparticles. The release of nanoparticles from ultrasound-driven, oscillating microbubbles features many new phenomena such as release of the payload at low pressure, transport of the released material in the flow field generated by the bubble, and directional particle release and "injection" across physiological barriers. In particular, the acoustic microstreaming flow generated by the bubbles can simultaneously increase the permeability of the cell membrane, and actively transport therapeutic agents, with a potential synergistic effect for enhanced drug delivery. There is potential to further exploit these phenomena to achieve more efficient drug delivery, provided that they can be controlled through acoustic pressure, frequency, and microbubble formulation. Future research in surface engineering of microbubbles should address the challenge of combining different types of therapeutic nanoparticles directly with the gas core of a microbubble; achieving sustained release through the choice of ultrasound parameters that lead to sufficiently small oscillations to avoid microbubble collapse, but sufficiently large

to promote particle expulsion; and controlling the transport of the payload through bubble dynamics for enhanced uptake.

Acknowledgement

The authors thank G. ter Haar and J. J. Choi for useful discussions. D. B. is supported by Newton International Fellowship No. NF161558. Support from the European Research Council, Starting Grant No. 639221 (V.G.) is also acknowledged.

References

(1) Klibanov, A. L. *Investigative radiology* **2006**, *41*, 354–362.

(2) Coussios, C. C.; Roy, R. A. *Annu. Rev. Fluid Mech.* **2008**, *40*, 395–420.

(3) Amreddy, N.; Babu, A.; Muralidharan, R.; Panneerselvam, J.; Srivastava, A.; Ahmed, R.; Mehta, M.; Munshi, A.; Ramesh, R. In *Recent Advances in Nanoparticle-Based Cancer Drug and Gene Delivery*; Tew, K. D., Fisher, P. B., Eds.; Advances in Cancer Research; Academic Press, 2018; Vol. 137; pp 115 – 170.

(4) Yang, F.; Li, Y.; Chen, Z.; Zhang, Y.; Wu, J.; Gu, N. *Biomaterials* **2009**, *30*, 3882 – 3890.

(5) Yang, F.; Zhang, M.; He, W.; Chen, P.; Cai, X.; Yang, L.; Gu, N.; Wu, J. *Small* **2011**, *7*, 902–910.

(6) Chertok, B.; Langer, R. *Theranostics* **2018**, *8*, 341.

(7) Zhao, X.; Quinto-Su, P. A.; Ohl, C.-D. *Phys. Rev. Lett.* **2009**, *102*, 024501.

(8) Mulvana, H.; Eckersley, R. J.; Tang, M.-X.; Pankhurst, Q.; Stride, E. *Ultrasound Med. Biol.* **2012**, *38*, 864–875.

(9) Gao, Y.; Chan, C. U.; Gu, Q.; Lin, X.; Zhang, W.; Yeo, D. C. L.; Alsema, A. M.; Arora, M.; Chong, M. S. K.; Shi, P.; Ohl, C.-D.; Xu, C. *NPG Asia Mater.* **2016**, *8*, e260.

(10) Lentacker, I.; De Smedt, S. C.; Sanders, N. N. *Soft Matter* **2009**, *5*, 2161.

(11) Borden, M. A.; Song, K.-H. *Advances in Colloid and Interface Science* **2018**,

(12) Qin, S.; Caskey, C. F.; Ferrara, K. W. *Physics in Medicine and Biology* **2009**, *54*.

(13) Errico, C.; Pierre, J.; Pezet, S.; Desailly, Y.; Lenkei, Z.; Couture, O.; Tanter, M. *Nature* **2015**, *527*, 499–502.

(14) Helfield, B.; Chen, X.; Watkins, S. C.; Villanueva, F. S. *Proceedings of the National Academy of Sciences* **2016**, *113*, 9983–9988.

(15) Tachibana, K.; Tachibana, S. *Circulation* **1995**, *92*, 1148–50.

(16) Jiang, N.; Xie, B.; Zhang, X.; He, M.; Li, K.; Bai, J.; Wang, Z.; He, J.; Zhang, L. *Cardiovascular and Interventional Radiology* **2014**, *37*, 1321–1328.

(17) Sheikov, N.; McDannold, N.; Vykhodtseva, N.; Jolesz, F.; Hynynen, K. *Ultrasound in Medicine & Biology* **2004**, *30*, 979–989.

(18) Ferrara, K. W.; Borden, M. A.; Zhang, H. *Accounts of Chemical Research* **2009**, *42*, 881–892.

(19) Ja'afar, F.; Leow, C. H.; Garbin, V.; Sennoga, C. A.; Tang, M.-X.; Seddon, J. M. *Ultrasound in Medicine & Biology* **2015**, *41*, 2990 – 3000.

(20) Lum, A. F.; Borden, M. A.; Dayton, P. A.; Kruse, D. E.; Simon, S. I.; Ferrara, K. W. *Journal of Controlled Release* **2006**, *111*, 128–134.

(21) Lentacker, I.; De Cock, I.; Deckers, R.; De Smedt, S. C.; Moonen, C. T. W. *Advanced Drug Delivery Reviews* **2014**, *72*, 49–64.

(22) Kudo, N.; Okada, K.; Yamamoto, K. *Biophysical Journal* **2009**, *96*, 4866–4876.

(23) Lai, C.-Y.; Wu, C.-H.; Chen, C.-C.; Li, P.-C. *Ultrasound in medicine & biology* **2006**, *32*, 1931–1941.

(24) Liang, H. D.; Tang, J.; Halliwell, M. *Proceedings of the Institution of Mechanical Engineers, Part H: Journal of Engineering in Medicine* **2010**, *224*, 343–361.

(25) van Wamel, A.; Kooiman, K.; Harteveld, M.; Emmer, M.; ten Cate, F. J.; Versluis, M.; de Jong, N. *Journal of Controlled Release* **2006**, *112*, 149–155.

(26) Pereno, V.; Aron, M.; Vince, O.; Mannaris, C.; Seth, A.; De Saint Victor, M.; Lajoinie, G.; Versluis, M.; Coussios, C.; Carugo, D.; Stride, E. *Biomicrofluidics* **2018**, *12*.

(27) Bolaños-Jiménez, R.; Rossi, M.; Rivas, D. F.; Kähler, C. J.; Marin, A. *Journal of Fluid Mechanics* **2017**, *820*, 529–548.

(28) Zhou, Y.; Yang, K.; Cui, J.; Ye, J. Y.; Deng, C. X. *Journal of Controlled Release* **2012**, *157*, 103–111.

(29) Meijering, B. D.; Juffermans, L. J.; van Wamel, A.; Henning, R. H.; Zuhorn, I. S.; Emmer, M.; Versteilen, A. M.; Paulus, W. J.; van Gilst, W. H.; Kooiman, K.; de Jong, N.; Musters, R. J.; Deelman, L. E.; Kamp, O. *Circulation Research* **2009**, *104*, 679–687.

(30) De Cock, I.; Zagato, E.; Braeckmans, K.; Luan, Y.; de Jong, N.; De Smedt, S. C.; Lentacker, I. *Journal of controlled release : official journal of the Controlled Release Society* **2015**, *197*, 20–28.

(31) De Cock, I.; Lajoinie, G.; Versluis, M.; De Smedt, S. C.; Lentacker, I. *Biomaterials* **2016**, *83*, 294–307.

(32) Butler, B. D.; Hills, B. A. *Journal of Applied Physiology* **1979**, *47*, 537–543.

(33) Klibanov, A. L. In *Contrast Agents II: Optical, Ultrasound, X-Ray and Radiopharmaceutical Imaging*; Krause, W., Ed.; Topics in Current Chemistry; Springer Berlin Heidelberg: Berlin, Heidelberg, 2002; pp 73–106.

(34) Barak, M.; Katz, Y. *Chest* **2005**, *128*, 2918–2932.

(35) Feinstein, S. B.; Cheirif, J.; Ten Cate, F. J.; Silverman, P. R.; Heidenreich, P. A.; Dick, C.; Desir, R. M.; Armstrong, W. F.; Quinones, M. A.; Shah, P. M. *Journal of the American College of Cardiology* **1990**, *16*, 316–324.

(36) Cosgrove, D. *European Journal of Radiology* **2006**, *60*, 324–330.

(37) Calliada, F.; Campani, R.; Bottinelli, O.; Bozzini, A.; Sommaruga, M. G. *European Journal of Radiology* **1998**, *27*, S157–S160.

(38) Garbin, V. *The Micro-World Observed by Ultra High-Speed Cameras*; Springer, 2018; pp 357–374.

(39) Borden, M. A.; Pu, G.; Runner, G. J.; Longo, M. L. *Colloids and Surfaces B: Biointerfaces* **2004**, *35*, 209–223.

(40) Fuller, G. G.; Vermant, J. *Ann. Rev. Chem. Biomol. Engi.* **2012**, *3*, 519–543.

(41) Tsigklifis, K.; Pelekasis, N. A. *Physics of Fluids* **2013**, *25*, 032109.

(42) Sarkar, K.; Shi, W. T.; Chatterjee, D.; Forsberg, F. *J. Acoust. Soc. Am.* **2005**, *118*, 539–550.

(43) Chatterjee, D.; Sarkar, K. *Ultrasound Med. Biol.* **2003**, *29*, 1749–1757.

(44) Duncan, P. B.; Needham, D. *Langmuir* **2004**, *20*, 2567–2578.

(45) Borden, M. A.; Longo, M. L. *Langmuir* **2002**, *18*, 9225–9233.

(46) Pu, G.; Borden, M. A.; Longo, M. L. *Langmuir* **2006**, *22*, 2993–2999.

(47) Hanwright, J.; Zhou, J.; Evans, G. M.; Galvin, K. P. *Langmuir* **2005**, *21*, 4912–4920.

(48) Katiyar, A.; Sarkar, K.; Jain, P. *Journal of Colloid and Interface Science* **2009**, *336*, 519–525.

(49) Sarkar, K.; Katiyar, A.; Jain, P. *Ultrasound in medicine & biology* **2009**, *35*, 1385–1396.

(50) Murray, B. S.; Ettelaie, R. *Current opinion in colloid & interface science* **2004**, *9*, 314–320.

(51) Stocco, A.; Rio, E.; Binks, B. P.; Langevin, D. *Soft Matter* **2011**, *7*, 1260–1267.

(52) Yasui, K.; Tuziuti, T.; Kanematsu, W.; Kato, K. *Langmuir* **2016**, *32*, 11101–11110.

(53) Lee, M.; Yeol Lee, E.; Lee, D.; Jun Park, B. *Soft Matter* **2015**, *11*, 2067–2079.

(54) Xu, Q.; Nakajima, M.; Ichikawa, S.; Nakamura, N.; Shiina, T. *Innovative Food Science & Emerging Technologies* **2008**, *9*, 489–494.

(55) Unger, E.; McCreery, T.; Yellowhair, D.; Barrette, T. R. Apparatus and Method for Making Gas-Filled Vesicles of Optimal Size. 1997.

(56) Feinstein, S. B.; Cate, F. J. T.; Zwehl, W.; Ong, K.; Maurer, G.; Tei, C.; Shah, P. M.; Meerbaum, S.; Corday, E. *Journal of the American College of Cardiology* **1984**, *3*, 14–20.

(57) Keller, M. W.; Feinstein, S. B.; Briller, R. A.; Powsner, S. M. *Journal of Ultrasound in Medicine* **1986**, *5*, 493–498.

(58) Grinstaff, M. W.; Suslick, K. S. *Proceedings of the National Academy of Sciences* **1991**, *88*, 7708–7710.

(59) Borrelli, M. J.; O'Brien, W. D.; Bernock, L. J.; Williams, H. R.; Hamilton, E.; Wu, J.; Oelze, M. L.; Culp, W. C. *Ultrasonics Sonochemistry* **2012**, *19*, 198–208.

(60) Mahalingam, S.; Meinders, M. B. J.; Edirisinghe, M. *Langmuir* **2014**, *30*, 6694–6703.

(61) Mahalingam, S.; Raimi-Abraham, B. T.; Craig, D. Q. M.; Edirisinghe, M. *Langmuir* **2015**, *31*, 659–666.

(62) Feshitan, J. A.; Chen, C. C.; Kwan, J. J.; Borden, M. A. *Journal of Colloid and Interface Science* **2009**, *329*, 316–324.

(63) Kok, M. P.; Segers, T.; Versluis, M. *Lab Chip* **2015**, *15*, 3716–3722.

(64) Segers, T.; Versluis, M. *Lab on a Chip* **2014**, *14*, 1705–1714.

(65) Stride, E.; Edirisinghe, M. *Soft Matter* **2008**, *4*, 2350–2359.

(66) Huerre, A.; Miralles, V.; Jullien, M.-C. *Soft Matter* **2014**, *10*, 6888–6902.

(67) Anna, S. L. *Annual Review of Fluid Mechanics* **2016**, *48*, 285–309.

(68) Garstecki, P.; J. Fuerstman, M.; A. Stone, H.; M. Whitesides, G. *Lab on a Chip* **2006**, *6*, 437–446.

(69) Anna, S. L.; Bontoux, N.; Stone, H. A. *Applied Physics Letters* **2003**, *82*, 364–366.

(70) Menech, M. D.; Garstecki, P.; Jousse, F.; Stone, H. A. *Journal of Fluid Mechanics* **2008**, *595*, 141–161.

(71) van Steijn, V.; R. Kleijn, C.; T. Kreutzer, M. *Lab on a Chip* **2010**, *10*, 2513–2518.

(72) Chen, C.; Zhu, Y.; Leech, P. W.; Manasseh, R. *Applied Physics Letters* **2009**, *95*, 144101.

(73) Hettiarachchi, K.; Talu, E.; L. Longo, M.; A. Dayton, P.; P. Lee, A. *Lab on a Chip* **2007**, *7*, 463–468.

(74) Peyman, S. A.; Abou-Saleh, R. H.; McLaughlan, J. R.; Ingram, N.; Johnson, B. R.; Critchley, K.; Freear, S.; Anthony Evans, J.; F. Markham, A.; Louise Coletta, P.; D. Evans, S. *Lab on a Chip* **2012**, *12*, 4544–4552.

(75) van Hoeve, W.; Dollet, B.; Gordillo, J. M.; Versluis, M.; van Wijngaarden, L.; Lohse, D. *EPL (Europhysics Letters)* **2011**, *94*, 64001.

(76) Cubaud, T.; Tatineni, M.; Zhong, X.; Ho, C.-M. *Physical Review E* **2005**, *72*, 037302.

(77) Stride, E.; Edirisinghe, M. *Medical & Biological Engineering & Computing* **2009**, *47*, 883–892.

(78) Lee, M. H.; Prasad, V.; Lee, D. *Langmuir* **2010**, *26*, 2227–2230.

(79) Garbin, V.; Crocker, J. C.; Stebe, K. J. *Journal of Colloid and Interface Science* **2012**, *387*, 1 – 11.

(80) Brugarolas, T.; Park, B. J.; Lee, M. H.; Lee, D. *Advanced Functional Materials* **2011**, *21*, 3924–3931.

(81) Pancholi, K.; Stride, E.; Edirisinghe, M. *Langmuir* **2008**, *24*, 4388–4393.

(82) Mohamedi, G.; Azmin, M.; Pastoriza-Santos, I.; Huang, V.; Pérez-Juste, J.; Liz-Marzán, L. M.; Edirisinghe, M.; Stride, E. *Langmuir* **2012**, *28*, 13808–13815.

(83) Seo, M.; Gorelikov, I.; Williams, R.; Matsuura, N. *Langmuir* **2010**, *26*, 13855–13860.

(84) Owen, J.; Crake, C.; Lee, J. Y.; Carugo, D.; Beguin, E.; Khrapitchev, A. A.; Browning, R. J.; Sibson, N.; Stride, E. *Drug Delivery and Translational Research* **2018**, *8*, 342–356.

(85) Kothandaraman, A.; Harker, A.; Ventikos, Y.; Edirisinghe, M. *Micromachines* **2018**, *9*, 497.

(86) Dollet, B.; Marmottant, P.; Garbin, V. *Annual Review of Fluid Mechanics* **2019**, *51*, 331–355.

(87) Plesset, M. S.; Prosperetti, A. *Annual Review of Fluid Mechanics* **1977**, *9*, 145–185.

(88) Prosperetti, A. *The Journal of the Acoustical Society of America* **1977**, *61*, 17–27.

(89) Leighton, T. *The acoustic bubble*; Academic press, 1997.

(90) de Jong, N.; Hoff, L.; Skotland, T.; Bom, N. *Ultrasonics* **1992**, *30*, 95–103.

(91) Church, C. C. *J. Acoust. Soc. Am.* **1995**, *97*, 1510–1521.

(92) Marmottant, P.; van der Meer, S.; Emmer, M.; Versluis, M.; de Jong, N.; Hilgenfeldt, S.; Lohse, D. *J. Acoust. Soc. Am.* **2005**, *118*, 3499–3505.

(93) van der Meer, S. M.; Dollet, B.; Voormolen, M. M.; Chin, C. T.; Bouakaz, A.; de Jong, N.; Versluis, M.; Lohse, D. *J. Acoust. Soc. Am.* **2007**, *121*, 648–656.

(94) Razavi, S.; Cao, K. D.; Lin, B.; Lee, K. Y. C.; Tu, R. S.; Kretzschmar, I. *Langmuir* **2015**, *31*, 7764–7775.

(95) Versluis, M.; Goertz, D. E.; Palanchon, P.; Heitman, I. L.; van der Meer, S. M.; Dollet, B.; de Jong, N.; Lohse, D. *Phys. Rev. E* **2010**, *82*, 026321.

(96) Dollet, B.; van der Meer, S. M.; Garbin, V.; de Jong, N.; Lohse, D.; Versluis, M. *Ultrasound Med. Biol.* **2008**, *34*, 1465–1473.

(97) Poulichet, V.; Huerre, A.; Garbin, V. *Soft Matter* **2017**, 125–133.

(98) Lighthill, J. *Journal of sound and vibration* **1978**, *61*, 391–418.

(99) Nyborg, W. *The British journal of cancer. Supplement* **1982**, *5*, 156.

(100) Elder, S. A. *The Journal of the Acoustical Society of America* **1959**, *31*, 54–64.

(101) Nyborg, W. L. *The Journal of the Acoustical Society of America* **1958**, *30*, 329–339.

(102) Watson, Y. E.; Birkin, P. R.; Leighton, T. G. *Ultrasonics Sonochemistry* **2003**, *10*, 65–69.

(103) Tho, P.; Manasseh, R.; Ooi, A. *Journal of Fluid Mechanics* **2007**, *576*, 191.

(104) Rooney, J. A. *The Journal of the Acoustical Society of America* **1972**, *52*, 1718–1724.

(105) Marmottant, P.; Hilgenfeldt, S. *Nature* **2003**, *423*, 153–156.

(106) Pommella, A.; Brooks, N. J.; Seddon, J. M.; Garbin, V. *Scientific reports* **2015**, *5*, 13163.

(107) Luan, Y.; Lajoinie, G.; Gelderblom, E.; Skachkov, I.; van der Steen, A. F. W.; Vos, H. J.; Versluis, M.; De Jong, N. *Ultrasound in Medicine and Biology* **2014**, *40*, 1834–1846.

(108) Lajoinie, G.; Luan, Y.; Gelderblom, E.; Dollet, B.; Mastik, F.; Dewitte, H.; Lentacker, I.; de Jong, N.; Versluis, M. *Communications Physics* **2018**, *1*, 22.

(109) Poulichet, V.; Garbin, V. *Proc. Natl. Acad. Sci. USA* **2015**, *112*, 5932–5937.

(110) Sijl, J.; Overvelde, M.; Dollet, B.; Garbin, V.; de Jong, N.; Lohse, D.; Versluis, M. *J. Acoust. Soc. Am.* **2011**, *129*, 1729–1739.

(111) Binks, B. P. *Current opinion in colloid & interface science* **2002**, *7*, 21–41.

Graphical TOC Entry